Chapter 2
Single Wind Turbine Power Generation Systems

Abstract For a power system with substantial power generation from wind farms, controllability of the wind farm power outputs is critical to power system reliability and economy. Both the active and reactive powers need to be maintained at appropriate levels. Indeed, recent experience with wind farm operation and research suggests that a wind farm should have at least two operating modes: *maximum power tracking* (MPT) and *power regulation* (PR). MPT is a traditional operating mode, aimed at enabling wind turbines in a wind farm to convert as much of the energy in wind to electrical energy as possible under normal operation conditions. PR, on the other hand, is concerned with adjusting the wind turbine power outputs as needed by power system reliability, or economic conditions. Being able to operate in either the MPT or PR mode is becoming increasingly important as the penetration of wind energy increases. In this chapter, we first introduce the basic structure of and a mathematical model for a variable-speed wind turbine with a doubly fed induction generator (DFIG), a widely used power generation technology today. This model may be used in the development of controllers for controlling the active and reactive power outputs of the wind turbine. Indeed, we also illustrate an application of the model to the design of a reconfigurable nonlinear controller, which enables the wind turbine to maximize its active power in the MPT mode, regulate its active power in the PR mode, switch between the two modes, and adjust its reactive power to achieve a desired power factor, while coping with uncertainties in most of its parameters. Finally, we demonstrate the effectiveness of the controller through simulation with a realistic wind profile.

2.1 Introduction

The basic structure of a typical variable-speed wind turbine with a DFIG is shown in Fig. 2.1. The DFIG is an electric generator employed in most variable-speed wind turbines, which is a three-phase slip-ring induction machine, with its stator windings directly connected to the power grid, and its rotor windings connected to the grid through a bidirectional four-quadrant power electronic converter which can vary the frequency, magnitude, and phases of the voltage, or current, in the rotor windings. The

© Springer International Publishing Switzerland 2016

J.N. Jiang et al., *Control and Operation of Grid-Connected Wind Farms*,
Advances in Industrial Control, DOI 10.1007/978-3-319-39135-9_2

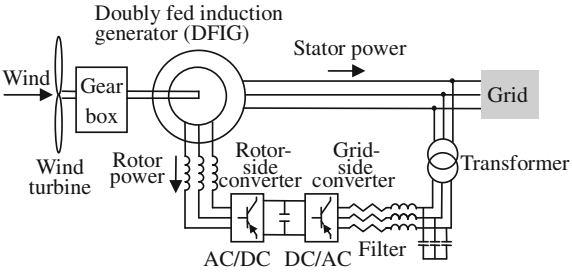


Fig. 2.1 Basic structure of a typical variable-speed wind turbine with a DFIG

wind turbine is of a variable blade pitch angle type, whose aerodynamic properties are characterized by a family of performance coefficient curves also known as C_p-curves or C_p-surface. Typically, a fixed ratio gearbox is used to couple the wind turbine and the DFIG. The gearbox, however, is usually ignored in many studies on wind turbine control, and this monograph is no exception.

In general, both the stator and rotor windings are three-phase circuits. In this monograph, the analysis of two three-phase circuits, including the electrical variables such as voltages, currents, and impedances, will be carried out using the synchronously rotating direct-quadrature axis (dq-axis) frame, where the relationship between three-phase quantities and dq components is given in terms of the direct–quadrature–zero (or $dq0$) transformation and its inverse [15]. In a typical implementation for balanced three-phase circuits of stators and rotors, the dq analysis is based on a synchronously rotating dq-axis frame, where the d-axis is oriented along the stator-flux vector position. The study can then be carried out and implemented using vector control in the stator-flux orientation to achieve a decoupled control between electrical torque and rotor excitation voltage or current. In the dq-axis frame, independent control of the active and reactive power outputs can be achieved, just as in the case of a synchronous generator, so the analysis and design of controllers can be carried out succinctly without losing any generality.

Furthermore, in the analysis and design of control algorithms, we assume that the rotor-side circuit, including the rotor-side converter, grid-side convertor, capacitor, and transformer as shown in Fig. 2.1, are ideal. We also assume that any control algorithm for the voltages and currents of the rotor windings can be physically realized.

2.2 Mathematical Model

2.2.1 Electrical Dynamics

Consider a variable-speed wind turbine with a DFIG, as shown in Fig. 2.1. For this wind turbine, the dynamics of its electrical part can be represented by a fourth-order state space model. To see this, note that the voltage equations are [38]

$$v_{ds} = R_s i_{ds} - \omega_s \varphi_{qs} + \dot{\varphi}_{ds}, \tag{2.1}$$
$$v_{qs} = R_s i_{qs} + \omega_s \varphi_{ds} + \dot{\varphi}_{qs}, \tag{2.2}$$
$$v_{dr} = R_r i_{dr} - (\omega_s - \omega_r)\varphi_{qr} + \dot{\varphi}_{dr}, \tag{2.3}$$
$$v_{qr} = R_r i_{qr} + (\omega_s - \omega_r)\varphi_{dr} + \dot{\varphi}_{qr}, \tag{2.4}$$

where $v_{ds}, v_{qs}, v_{dr}, v_{qr} \in \mathbb{R}$ are the d- and q-axis components of the stator and rotor voltages; $i_{ds}, i_{qs}, i_{dr}, i_{qr} \in \mathbb{R}$ are the d- and q-axis components of the stator and rotor currents; $\varphi_{ds}, \varphi_{qs}, \varphi_{dr}, \varphi_{qr} \in \mathbb{R}$ are the d- and q-axis components of the stator and rotor fluxes; $\omega_s > 0$ is the constant angular velocity of the synchronously rotating reference frame; $\omega_r > 0$ is the rotor angular velocity; and R_s, R_r are the stator and rotor resistances. The flux equations are [38]

$$\varphi_{ds} = L_s i_{ds} + L_m i_{dr}, \tag{2.5}$$
$$\varphi_{qs} = L_s i_{qs} + L_m i_{qr}, \tag{2.6}$$
$$\varphi_{dr} = L_m i_{ds} + L_r i_{dr}, \tag{2.7}$$
$$\varphi_{qr} = L_m i_{qs} + L_r i_{qr}, \tag{2.8}$$

where L_s, L_r, and L_m are the stator, rotor, and mutual inductances, respectively, satisfying $L_s > L_m$ and $L_r > L_m$. From (2.5)–(2.8), the current equations can be written as

$$i_{ds} = \frac{1}{\sigma L_s}\varphi_{ds} - \frac{L_m}{\sigma L_s L_r}\varphi_{dr}, \tag{2.9}$$
$$i_{qs} = \frac{1}{\sigma L_s}\varphi_{qs} - \frac{L_m}{\sigma L_s L_r}\varphi_{qr}, \tag{2.10}$$
$$i_{dr} = -\frac{L_m}{\sigma L_s L_r}\varphi_{ds} + \frac{1}{\sigma L_r}\varphi_{dr}, \tag{2.11}$$
$$i_{qr} = -\frac{L_m}{\sigma L_s L_r}\varphi_{qs} + \frac{1}{\sigma L_r}\varphi_{qr}, \tag{2.12}$$

where $\sigma = 1 - L_m^2/(L_s L_r)$ is the leakage coefficient. Selecting the four fluxes as state variables and substituting (2.9)–(2.12) into (2.1)–(2.4), the electrical dynamics in state space form can be written as

$$\dot{\varphi}_{ds} = -\frac{R_s}{\sigma L_s}\varphi_{ds} + \omega_s \varphi_{qs} + \frac{R_s L_m}{\sigma L_s L_r}\varphi_{dr} + v_{ds}, \tag{2.13}$$
$$\dot{\varphi}_{qs} = -\omega_s \varphi_{ds} - \frac{R_s}{\sigma L_s}\varphi_{qs} + \frac{R_s L_m}{\sigma L_s L_r}\varphi_{qr} + v_{qs}, \tag{2.14}$$
$$\dot{\varphi}_{dr} = \frac{R_r L_m}{\sigma L_s L_r}\varphi_{ds} - \frac{R_r}{\sigma L_r}\varphi_{dr} + (\omega_s - \omega_r)\varphi_{qr} + v_{dr}, \tag{2.15}$$
$$\dot{\varphi}_{qr} = \frac{R_r L_m}{\sigma L_s L_r}\varphi_{qs} - (\omega_s - \omega_r)\varphi_{dr} - \frac{R_r}{\sigma L_r}\varphi_{qr} + v_{qr}. \tag{2.16}$$

Treating the rotor voltages v_{dr} and v_{qr} as control variables and the stator voltages v_{ds} and v_{qs} as constants (that are not simultaneously zero), the dynamics (2.13)–(2.16) can be written in a matrix form as

$$\begin{bmatrix} \dot{\varphi}_{ds} \\ \dot{\varphi}_{qs} \\ \dot{\varphi}_{dr} \\ \dot{\varphi}_{qr} \end{bmatrix} = \underbrace{\begin{bmatrix} -\frac{R_s}{\sigma L_s} & \omega_s & \frac{R_s L_m}{\sigma L_s L_r} & 0 \\ -\omega_s & -\frac{R_s}{\sigma L_s} & 0 & \frac{R_s L_m}{\sigma L_s L_r} \\ \frac{R_r L_m}{\sigma L_s L_r} & 0 & -\frac{R_r}{\sigma L_r} & \omega_s \\ 0 & \frac{R_r L_m}{\sigma L_s L_r} & -\omega_s & -\frac{R_r}{\sigma L_r} \end{bmatrix}}_{A} \begin{bmatrix} \varphi_{ds} \\ \varphi_{qs} \\ \varphi_{dr} \\ \varphi_{qr} \end{bmatrix} + \underbrace{\begin{bmatrix} 0 & 0 \\ 0 & 0 \\ 1 & 0 \\ 0 & 1 \end{bmatrix}}_{B} \begin{bmatrix} v_{dr} \\ v_{qr} \end{bmatrix} + \begin{bmatrix} v_{ds} \\ v_{qs} \\ -\omega_r \varphi_{qr} \\ \omega_r \varphi_{dr} \end{bmatrix}, \tag{2.17}$$

where A and B are constant matrices as defined in (2.17). Similarly, the flux–current relationship (2.5)–(2.8) can be written in a matrix form as

$$\underbrace{\begin{bmatrix} \varphi_{ds} \\ \varphi_{qs} \\ \varphi_{dr} \\ \varphi_{qr} \end{bmatrix}}_{\varphi} = \begin{bmatrix} L_s & 0 & L_m & 0 \\ 0 & L_s & 0 & L_m \\ L_m & 0 & L_r & 0 \\ 0 & L_m & 0 & L_r \end{bmatrix} \underbrace{\begin{bmatrix} i_{ds} \\ i_{qs} \\ i_{dr} \\ i_{qr} \end{bmatrix}}_{i}, \tag{2.18}$$

where φ and i are vectors as defined in (2.18).

Neglecting power losses associated with stator and rotor resistances, the active and reactive stator and rotor powers are given by [68]

$$P_s = -v_{ds} i_{ds} - v_{qs} i_{qs}, \tag{2.19}$$
$$Q_s = -v_{qs} i_{ds} + v_{ds} i_{qs}, \tag{2.20}$$
$$P_r = -v_{dr} i_{dr} - v_{qr} i_{qr}, \tag{2.21}$$
$$Q_r = -v_{qr} i_{dr} + v_{dr} i_{qr}, \tag{2.22}$$

and the total active and reactive powers of the turbine are

$$P = P_s + P_r, \tag{2.23}$$
$$Q = Q_s + Q_r, \tag{2.24}$$

where positive (negative) values of P and Q mean that the turbine injects power into (draws power from) the power grid.

2.2.2 *Mechanical Dynamics*

The dynamics of the mechanical part of the wind turbine can be represented by a first-order state space model [15]

$$J\dot{\omega}_r = T_m - T_e - C_f\omega_r, \tag{2.25}$$

where the rotor angular velocity ω_r is another state variable, J is the moment of inertia, C_f is the friction coefficient, T_m is the mechanical torque generated, and T_e is the electromagnetic torque which can be expressed as [68]

$$T_e = \varphi_{qs} i_{ds} - \varphi_{ds} i_{qs}, \tag{2.26}$$

where a positive (negative) value of T_e corresponds to the turbine acting as a generator (motor). It is known that [14] the mechanical power P_m converted from wind through the turbine blades is given by

$$P_m = T_m\omega_r = \frac{1}{2}\rho A C_p(\lambda, \beta) V_w^3, \tag{2.27}$$

where ρ is the air density, $A = \pi R^2$ is the area swept by the rotor blades of radius R, V_w is the wind speed, and $C_p(\lambda, \beta)$, commonly referred to as the C_p-surface, is the performance coefficient of the wind turbine, whose value is a function of the tip speed ratio $\lambda \in (0, \infty)$, defined as

$$\lambda = \frac{\omega_r R}{V_w}, \tag{2.28}$$

and the blade pitch angle $\beta \in [\beta_{\min}, \beta_{\max}]$, which is another control variable.

The performance coefficient $C_p(\lambda, \beta)$ is typically provided by turbine manufacturers and may vary greatly from one turbine to another [14]. Therefore, to make the results of this chapter broadly applicable to a wide variety of turbines, no specific expression of $C_p(\lambda, \beta)$ will be assumed. Instead, $C_p(\lambda, \beta)$ will only be assumed to satisfy the following mild assumptions for the purpose of analysis:

A1. Function $C_p(\lambda, \beta)$ is continuously differentiable in both λ and β over $\lambda \in (0, \infty)$ and $\beta \in [\beta_{\min}, \beta_{\max}]$.

A2. There exists $c \in (0, \infty)$ such that for all $\lambda \in (0, \infty)$ and $\beta \in [\beta_{\min}, \beta_{\max}]$, we have $C_p(\lambda, \beta) \le c\lambda$. This assumption is mild because it is equivalent to saying that the mechanical torque T_m is bounded from above, since $T_m \propto \frac{C_p(\lambda,\beta)}{\lambda}$ according to (2.27) and (2.28).

A3. For each fixed $\beta \in [\beta_{\min}, \beta_{\max}]$, there exists $\lambda_1 \in (0, \infty)$ such that for all $\lambda \in (0, \lambda_1)$, we have $C_p(\lambda, \beta) > 0$. This assumption is also mild because turbines are designed to capture wind power over a wide range of λ, including times when λ is small.

A4. There exist $\underline{c} \in (-\infty, 0)$ and $\overline{c} \in (0, \infty)$ such that for all $\lambda \in (0, \infty)$ and $\beta \in [\beta_{\min}, \beta_{\max}]$, we have $\underline{c} \le \frac{\partial}{\partial\lambda}(\frac{C_p(\lambda,\beta)}{\lambda}) \le \overline{c}$.

As it follows from the above, the wind turbine is modeled as a fifth-order nonlinear dynamical system with state variables φ_{ds}, φ_{qs}, φ_{dr}, φ_{qr}, and ω_r; control variables v_{dr}, v_{qr}, and β; output variables P and Q; exogenous "disturbance" V_w;

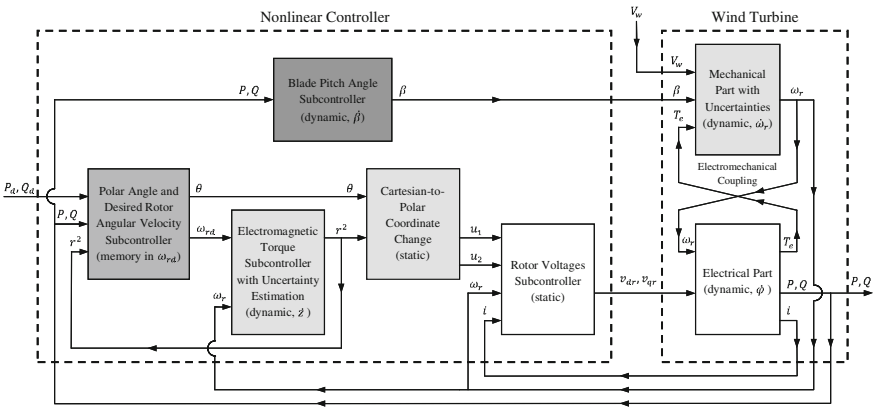


Fig. 2.2 Block diagram of the wind turbine and the nonlinear dual-mode controller

nonlinear state equations (2.17) and (2.25); and nonlinear output equations (2.19)–(2.24). Notice that the system dynamics are strongly coupled: the mechanical state variable ω_r affects the electrical dynamics bilinearly via the third and fourth rows of (2.17) (i.e., (2.15) and (2.16)), while the electrical state variables φ_{ds}, φ_{qs}, φ_{dr}, and φ_{qr} affect the mechanical dynamics quadratically via (2.9)–(2.12), (2.25), and (2.26). Since the stator winding of the DFIG is directly connected to the grid, for reliability reasons the stator voltages v_{ds} and v_{qs} are assumed to be fixed and not to be controlled. Moreover, since (2.18) represents a bijective mapping between vectors φ and i and since the currents i and the rotor angular velocity ω_r can be measured, a controller for this system has access to all of its states (i.e., full state feedback is available). A block diagram of this system is shown on the right-hand side of Fig. 2.2, in which the electromechanical coupling can be seen.

In the rest of the chapter, we will illustrate an application of this wind turbine model to the design of a reconfigurable nonlinear controller. As will be shown, this controller not only allows the turbine to operate in either the MPT or PR mode by controlling its active and reactive powers via its rotor voltages and blade pitch angle, but also allows the turbine to have uncertainties in most of its parameters.

2.3 Nonlinear Dual-Mode Control with Uncertainties

Most grid-connected large-scale wind farms today operate in the *maximum power tracking* (MPT) mode, making their wind turbines harvest as much wind energy as possible, following the "let it be when the wind blows" philosophy of operation. With the current, relatively low level of wind energy penetration in the power generation portfolio, this MPT mode of operation does not cause significant issues. However, with the anticipated increase in penetration in the near future [2], MPT can negatively

impact power system reliability, such as producing excessive power that destabilizes a grid [1]. Thus, it is important that a wind farm can also operate in the so-called *power regulation* (PR) mode, whereby the total power output from its wind turbines is closely regulated at a desired setpoint, despite the fluctuating wind.

The ability of a wind farm to operate in either the MPT or PR mode, and switch seamlessly between them, is highly beneficial: not only does the PR mode provide a cushion to absorb the impact of wind fluctuations on the total power output, it also enables a power system to effectively respond to changes in reliability conditions and economic signals. For instance, when a sudden drop in load occurs, the power system may ask the wind farm to switch from MPT to PR and generate less power, rather than rely on expensive down-regulation generation. As another example, the PR mode, when properly designed, allows the total power output to smoothly and accurately follow system dispatch requests, thus reducing the reliance on ancillary services such as reliability reserves.

In the next section, we will develop a wind turbine controller with which a wind farm can have the aforementioned ability. More specifically, we will use the model from Sect. 2.2 to design a nonlinear dual-mode controller that controls the rotor voltages and blade pitch angle of a wind turbine, so that the turbine is capable of maximizing its active power in the MPT mode, regulating its active power in the PR mode, switching seamlessly between the two modes, adjusting its reactive power to achieve a desired power factor, and coping with inevitable uncertainties in most of its aerodynamic and mechanical parameters. The controller design will consist of the following steps: first, we show that although the dynamics of a wind turbine are highly nonlinear and electromechanically coupled, they possess a structure that makes the electrical part feedback linearizable, so that arbitrary pole placement can be carried out. We also show that because the electrical dynamics can be made very fast, it is possible to perform model order reduction, so that only the first-order mechanical dynamics remain to be considered. Next, we show that parametric uncertainties in the mechanical dynamics can be lumped and estimated via an uncertainty estimator which, together with a torque controller, enables the rotor angular velocity to track a desired reference whenever possible. Finally, we introduce a potential function that measures the difference between the actual and desired powers and present a gradient-like approach for minimizing this function.

We note that the current literature offers a large collection of wind turbine controllers, including [12, 27, 42, 43, 49, 52, 57–59, 65, 75, 77, 82, 87, 88, 95, 105, 108, 112–114]. However, most of the existing work consider the mechanical and electrical parts separately (e.g., [12, 27, 42, 43, 57–59, 82, 95, 105, 112] consider only the former, while [52, 65, 75, 77, 87, 88, 108, 113, 114] consider only the latter), and for a few of those (e.g., [49]) that consider both parts, its controller can only operate in the MPT mode as opposed to both the MPT and PR modes. Moreover, although the existing work has provided valuable understanding in the control of wind turbines, only a few address the issue of uncertainties. For example, [57–59] propose adaptive frameworks for controlling the mechanical part of wind turbines, so that the power captured is maximized, despite not knowing the turbine performance coefficient.

2.4 Controller Design

Given the model from Sect. 2.2, we address in this section the following problem: design a feedback controller that adjusts the rotor voltages v_{dr} and v_{qr} and blade pitch angle β, so that the active and reactive powers P and Q track—as closely as possible and limited only by wind strength—some time-varying desired references P_d and Q_d, presumably provided by a wind farm operator. When P_d is larger than what the wind turbine is capable of generating, it means that the operator wants the turbine to operate in the MPT mode; otherwise, the PR mode is sought. By also providing Q_d, the operator indirectly specifies a desired power factor $\text{PF}_d = P_d/\sqrt{P_d^2 + Q_d^2}$, around which the actual power factor $\text{PF} = P/\sqrt{P^2 + Q^2}$ should be regulated. The controller may use i, ω_r, P, and Q, which are all measurable, as feedback. The fluxes φ may also be viewed as feedback, since they are bijectively related to i through (2.18). Moreover, the controller may use values of all the electrical parameters (i.e., ω_s, R_s, R_r, L_s, L_r, L_m, v_{ds}, and v_{qs}) and turbine-geometry-dependent parameters (i.e., J, A, R, $\beta_{\min}$, and $\beta_{\max}$), since these values are typically quite accurately known. However, it may not use values of the C_p-surface, the air density ρ, and the friction coefficient C_f, since these values are inherently uncertain and can change over time. Furthermore, the controller should not rely on the wind speed V_w, since it may not be accurately measured.

Our solution to the above problem is a controller consisting of four subcontrollers. Figure 2.2 shows the architecture of this controller, in which the blocks represent its subcontrollers. Note that the controller accepts P_d and Q_d as reference inputs, uses i, ω_r, P, and Q as feedback, and produces v_{dr}, v_{qr}, and β as control inputs to the wind turbine. Moreover, the different gray levels of the blocks in Fig. 2.2 represent our intended timescale separation in the closed-loop dynamics: the darker a block, the slower its dynamics. The subcontrollers will be described in Sects. 2.4.1–2.4.4.

2.4.1 Rotor Voltages Subcontroller

Observe that although the electrical dynamics (2.17) are nonlinear, they possess a nice structure: the first and second rows of (2.17) are affine, consisting of linear terms and the constants v_{ds} and v_{qs}, while the third and fourth are nonlinear, consisting of linear terms, the control variables v_{dr} and v_{qr}, and the nonlinearities $-\omega_r\varphi_{qr}$ and $\omega_r\varphi_{dr}$ induced by the electromechanical coupling. Since the nonlinearities enter the dynamics the same way the control variables v_{dr} and v_{qr} do, we may use *feedback linearization* [62] to cancel them and perform *pole placement* [28], i.e., let

$$v_{dr} = \omega_r\varphi_{qr} - K_1^T\varphi + u_1, \tag{2.29}$$

$$v_{qr} = -\omega_r\varphi_{dr} - K_2^T\varphi + u_2, \tag{2.30}$$

where $\omega_r \varphi_{qr}$ and $-\omega_r \varphi_{dr}$ are intended to cancel the nonlinearities, $-K_1^T \varphi$ and $-K_2^T \varphi$ with $K_1, K_2 \in \mathbb{R}^4$ are for pole placement, and u_1 and u_2 are new control variables to be designed in Sect. 2.4.2.

Substituting (2.29) and (2.30) into (2.17), we obtain

$$\dot{\varphi} = (A - BK)\varphi + \begin{bmatrix} v_{ds} & v_{qs} & u_1 & u_2 \end{bmatrix}^T, \tag{2.31}$$

where $K = [K_1 \ K_2]^T$ is the state feedback gain matrix. Since the electrical dynamics are physically allowed to be much faster than the mechanicals, we may choose K in (2.31) to be such that $A - BK$ is asymptotically stable with very fast eigenvalues. With K chosen as such and with relatively slow-varying u_1 and u_2, the linear differential equation (2.31) may be approximated by a linear algebraic equation

$$\varphi = -(A - BK)^{-1} \begin{bmatrix} v_{ds} & v_{qs} & u_1 & u_2 \end{bmatrix}^T. \tag{2.32}$$

Consequently, the fifth-order state equations (2.17) and (2.25) may be approximated by the first-order state equation (2.25) along with algebraic relationships (2.29), (2.30), and (2.32). This approximation will be made in all subsequent development (but not in simulation).

Note that (2.18), (2.29), and (2.30) describe the *Rotor Voltages Subcontroller* block in Fig. 2.2.

2.4.2 *Electromagnetic Torque Subcontroller with Uncertainty Estimation*

Having addressed the electrical dynamics, we now consider the mechanicals, where the goal is to construct a subcontroller, which makes the rotor angular velocity ω_r track a desired, slow-varying reference ω_{rd}, despite not knowing most of the aerodynamic and mechanical parameters listed earlier.

To come up with such a subcontroller, we first introduce a coordinate change. As shown in [106], because of (2.18), (2.26), and (2.32), the electromagnetic torque T_e may be expressed as a quadratic function of the new control variables u_1 and u_2, i.e.,

$$T_e = \begin{bmatrix} u_1 & u_2 \end{bmatrix} \begin{bmatrix} q_1 & q_2 \\ q_2 & q_3 \end{bmatrix} \begin{bmatrix} u_1 \\ u_2 \end{bmatrix} + \begin{bmatrix} b_1 & b_2 \end{bmatrix} \begin{bmatrix} u_1 \\ u_2 \end{bmatrix} + a, \tag{2.33}$$

where q_1, q_2, q_3, b_1, b_2, and a depend on the electrical parameters and the state feedback gain matrix K. Moreover, as shown in Lemma 1 of [106], this quadratic function is always *strongly convex* because its associated Hessian matrix $\left[\begin{smallmatrix} q_1 & q_2 \\ q_2 & q_3 \end{smallmatrix}\right]$ is always *positive definite*. Since the mechanical dynamics (2.25), in ω_r, are driven by T_e, while T_e in (2.33) is a quadratic function of u_1 and u_2, the *two* new control variables u_1 and u_2 collectively affect *one* state variable ω_r. This implies that there

is a redundancy in u_1 and u_2, which may be exploited elsewhere. Since the quadratic function is always strongly convex, this redundancy may be exposed via the following coordinate change [106], which transforms $u_1, u_2 \in \mathbb{R}$ in a Cartesian coordinate system into $r \geq 0$ and $\theta \in [-\pi, \pi)$ in a polar coordinate system

$$r = \sqrt{z_1^2 + z_2^2}, \quad \theta = \text{atan2}(z_2, z_1), \tag{2.34}$$

where

$$\begin{bmatrix} z_1 \\ z_2 \end{bmatrix} = D^{1/2} M^T \begin{bmatrix} u_1 \\ u_2 \end{bmatrix} + \frac{1}{2} D^{-1/2} M^T \begin{bmatrix} b_1 \\ b_2 \end{bmatrix}, \tag{2.35}$$

$\text{atan2}(\cdot, \cdot)$ denotes the four-quadrant arctangent function, and M and D contain the eigenvectors and eigenvalues of $\left[\begin{smallmatrix} q_1 & q_2 \\ q_2 & q_3 \end{smallmatrix}\right]$ on their columns and diagonal, respectively, i.e.,

$$M^T \begin{bmatrix} q_1 & q_2 \\ q_2 & q_3 \end{bmatrix} M = D.$$

In the polar coordinates, it follows from (2.33)–(2.35) that

$$T_e = r^2 + a', \tag{2.36}$$

where $a' = -(v_{ds}^2 + v_{qs}^2)/(4\omega_s R_s)$ is always negative. From (2.25) and (2.36), we see that in the polar coordinates, r^2 is responsible for driving the mechanical dynamics in ω_r and, hence, may be viewed as an *equivalent electromagnetic torque*, differed from T_e only by a constant a'. On the other hand, the *polar angle* θ has no impact on the mechanical dynamics and, thus, represents the redundancy that will be exploited later, in Sect. 2.4.3.

Note that (2.34) and (2.35) describe the *Cartesian-to-Polar Coordinate Change* block in Fig. 2.2.

Having introduced the coordinate change, we next show that the unknown aerodynamic and mechanical parameters can be lumped into a scalar term, simplifying the problem. Combining (2.25), (2.27), (2.28), and (2.36),

$$J\dot{\omega}_r = \frac{\frac{1}{2}\rho A C_p(\frac{\omega_r R}{V_w}, \beta) V_w^3}{\omega_r} - r^2 - a' - C_f \omega_r. \tag{2.37}$$

Notice that the unknown parameters—namely, the C_p-surface, the air density ρ, the friction coefficient C_f, and the wind speed V_w—all appear in (2.37). Moreover, these unknown parameters can be separated from the "control input" r^2 and lumped into a scalar function $g(\omega_r, \beta, V_w)$, defined as

$$g(\omega_r, \beta, V_w) = \frac{\frac{1}{2}\rho A C_p(\frac{\omega_r R}{V_w}, \beta) V_w^3}{\omega_r} - a' - C_f \omega_r. \tag{2.38}$$

With $g(\omega_r, \beta, V_w)$ in (2.38) representing the aggregated uncertainties, the first-order dynamics (2.37) simplify to

$$\dot{\omega}_r = \frac{1}{J}(g(\omega_r, \beta, V_w) - r^2). \tag{2.39}$$

To design a controller for r^2, which allows the rotor angular velocity ω_r to track a desired, slow-varying reference ω_{rd} despite the unknown scalar function $g(\omega_r, \beta, V_w)$, consider a first-order nonlinear system

$$\dot{x} = \frac{1}{J}(f(x) + u), \tag{2.40}$$

where $x \in \mathbb{R}$ is the state, $u \in \mathbb{R}$ is the input, and $f(x)$ is a *known function* of x. Obviously, to drive x to some desired value $x_d \in \mathbb{R}$, we may apply feedback linearization [62] to cancel $f(x)$ and insert linear dynamics, i.e., let

$$u = -f(x) - \alpha(x - x_d), \tag{2.41}$$

where $\alpha \in \mathbb{R}$ is the controller gain. Combining (2.40) with (2.41) yields the closed-loop dynamics

$$\dot{x} = -\frac{\alpha}{J}(x - x_d). \tag{2.42}$$

Thus, if α is positive, x in (2.42) asymptotically goes to x_d.

Now suppose $f(x)$ in (2.40) is *unknown* but a *constant*, denoted simply as $f \in \mathbb{R}$ (we will relax the assumption that it is a constant shortly). With f being unknown, the controller (2.41) is no longer applicable. To overcome this limitation, we may first introduce a reduced-order estimator [17], which calculates an estimate $\widehat{f} \in \mathbb{R}$ of f, and then replace $f(x)$ in (2.41) by the estimate $\widehat{f}$

$$\dot{z} = -\frac{h}{J}(u + \widehat{f}), \tag{2.43}$$

$$\widehat{f} = z + hx, \tag{2.44}$$

$$u = -\widehat{f} - \alpha(x - x_d), \tag{2.45}$$

where $z \in \mathbb{R}$ is the estimator state and $h \in \mathbb{R}$ is the estimator gain. Defining the estimation error as $\widetilde{f} = f - \widehat{f}$ and combining (2.40) with (2.43)–(2.45) yield closed-loop dynamics

$$\dot{\widetilde{f}} = -\dot{\widehat{f}} = -\dot{z} - h\dot{x} = -\frac{h}{J}\widetilde{f}, \tag{2.46}$$

$$\dot{x} = \frac{1}{J}(f - \widehat{f} - \alpha(x - x_d)) = \frac{1}{J}(\widetilde{f} - \alpha(x - x_d)). \tag{2.47}$$

Hence, by letting both α and h be positive, both $\widetilde{f}$ and x in (2.46) and (2.47) asymptotically go to 0 and x_d, respectively.

Next, suppose both the state x and the desired value x_d must be *positive*, instead of being anywhere in $\mathbb{R}$. With this restriction, the controller with uncertainy estimation (2.43)–(2.45) needs to be modified, because for some initial conditions, it is possible that x can become nonpositive. One way to modify the controller is to replace the linear term $x - x_d$ in (2.45) by a logarithmic one $\ln(x/x_d)$, resulting in

$$u = -\widehat{f} - \alpha \ln \frac{x}{x_d}. \tag{2.48}$$

With (2.43), (2.44), and (2.48), the closed-loop dynamics become

$$\dot{\widetilde{f}} = -\frac{h}{J}\widetilde{f}, \tag{2.49}$$

$$\dot{x} = \frac{1}{J}(\widetilde{f} - \alpha \ln \frac{x}{x_d}). \tag{2.50}$$

Note from (2.50) that for any $\widetilde{f} \in \mathbb{R}$, there exists positive x, sufficiently small, such that $\dot{x}$ is positive. Therefore, for any initial condition $(\widetilde{f}(0), x(0))$ with positive $x(0)$, $x(t)$ will remain positive, suggesting that the modification (2.48) satisfies the restriction that both x and x_d must be positive.

Now suppose the input u must be *nonpositive*. With this additional restriction, (2.48) needs to be further modified. One way to do so is to force the right-hand side of (2.48) to be nonpositive, leading to

$$u = -\max\left\{\widehat{f} + \alpha \ln \frac{x}{x_d}, 0\right\}. \tag{2.51}$$

Clearly, with (2.51), u is always nonpositive.

Finally, suppose f is an *unknown function* of x, denoted as $f(x)$. With this relaxation, we may associate the first-order nonlinear system (2.40) with the first-order dynamics (2.39) by viewing x as ω_r, x_d as ω_{rd}, u as $-r^2$, $f(x)$ as $g(\omega_r, \beta, V_w)$ (treating β and V_w as constants), and $\widehat{f}$ as $\widehat{g}$ (i.e., $\widehat{g}$ is an estimate of $g(\omega_r, \beta, V_w)$). Based on this association, (2.43), (2.44), and (2.51) can be written as

$$\dot{z} = -\frac{h}{J}(-r^2 + \widehat{g}), \tag{2.52}$$

$$\widehat{g} = z + h\omega_r, \tag{2.53}$$

$$r^2 = \max\left\{\widehat{g} + \alpha \ln \frac{\omega_r}{\omega_{rd}}, 0\right\}. \tag{2.54}$$

Having derived the controller with uncertainty estimation (2.52)–(2.54), we now analyze its behavior. To do so, some setup is needed: first, suppose ω_{rd}, β, and V_w are constants. Second, as shown in Lemma 2 of [106], because of Assumptions A1–A3 in Sect. 2.2, there exists $\omega_r^{(1)} \in (0, \infty)$ such that $g(\omega_r^{(1)}, \beta, V_w) = 0$ and $g(\omega_r, \beta, V_w) > 0$ for all $\omega_r \in (0, \omega_r^{(1)})$. Third, using (2.28), (2.38), and Assumptions A1 and A4 in Sect. 2.2, it is straightforward to show that there exist $\underline{\gamma} \in (-\infty, 0)$ and $\overline{\gamma} \in (0, \infty)$ such that $\underline{\gamma} \leq \frac{\partial}{\partial \omega_r} g(\omega_r, \beta, V_w) \leq \overline{\gamma}$ for all $\omega_r \in (0, \infty)$. Finally, with (2.39) and (2.52)–(2.54) and with $(\omega_r, \widehat{g})$ as state variables (instead of (ω_r, z)), the closed-loop dynamics can be expressed as

$$\dot{\omega}_r = \frac{1}{J}\left(g(\omega_r, \beta, V_w) - \max\left\{\widehat{g} + \alpha \ln \frac{\omega_r}{\omega_{rd}}, 0\right\}\right), \tag{2.55}$$

$$\dot{\widehat{g}} = \dot{z} + h\dot{\omega}_r = \frac{h}{J}(g(\omega_r, \beta, V_w) - \widehat{g}). \tag{2.56}$$

The following theorem characterizes the stability properties of the closed-loop system (2.55) and (2.56), the proof of which can be found in [48]:

Theorem 2.1 *Consider the closed-loop system (2.55) and (2.56). Suppose ω_{rd}, β, and V_w are constants with $0 < \omega_{rd} \leq \omega_r^{(1)}$, where $\omega_r^{(1)}$, along with $\underline{\gamma}$ and $\overline{\gamma}$, is as defined above. Let $D = \{(\omega_r, \widehat{g}) | 0 < \omega_r \leq \omega_r^{(1)}, \widehat{g} \in \mathbb{R}\} \subset \mathbb{R}^2$. If the controller gain α is positive and estimator gain h is large enough, i.e.,*

$$\begin{aligned} &h > \overline{\gamma} \quad \text{if} \quad \overline{\gamma} \geq -\frac{1}{3}\underline{\gamma}, \\ &h > -\frac{(\overline{\gamma} - \underline{\gamma})^2}{8(\underline{\gamma} + \overline{\gamma})} \quad \text{otherwise}, \end{aligned} \tag{2.57}$$

then: (i) the system has a unique equilibrium point at $(\omega_{rd}, g(\omega_{rd}, \beta, V_w))$ in D; (ii) the set D is a positively invariant set, i.e., if $(\omega_r(0), \widehat{g}(0)) \in D$, then $(\omega_r(t), \widehat{g}(t)) \in D$ $\forall t \geq 0$; and (iii) the equilibrium point $(\omega_{rd}, g(\omega_{rd}, \beta, V_w))$ is locally asymptotically stable with a domain of attraction D.

Theorem 2.1 says that, by using the electromagnetic torque subcontroller with uncertainty estimation (2.52)–(2.54), if the gains α and h are positive and sufficiently large and if the desired reference ω_{rd} does not exceed $\omega_r^{(1)}$, then the rotor angular velocity ω_r asymptotically converges to ω_{rd} if ω_{rd}, β, and V_w are constants and closely tracks ω_{rd} if they are slow-varying. Notice that the gains α and h can be chosen independently of each other. Also, the condition "$\omega_{rd} \leq \omega_r^{(1)}$" is practically always satisfied, as $\omega_r^{(1)}$ is extremely large (see Fig. 3 of [106]).

Note that (2.52)–(2.54) describe the *Electromagnetic Torque Subcontroller with Uncertainty Estimation* block in Fig. 2.2.

2.4.3 Polar Angle and Desired Rotor Angular Velocity Subcontroller

Up to this point in the chapter, we have yet to specify how θ, ω_{rd}, and β are determined. To do so, we first introduce a scalar performance measure and express this measure as a function of θ, ω_{rd}, and β. We then present a method for choosing these variables, which optimizes the measure.

Recall that the ultimate goal is to make the active and reactive powers P and Q track some desired P_d and Q_d as closely as possible. Hence, it is useful to introduce a scalar performance measure, which characterizes how far P and Q are from P_d and Q_d. One such measure, denoted as U, is given by

$$U = \frac{1}{2}\begin{bmatrix} P - P_d & Q - Q_d \end{bmatrix}\begin{bmatrix} w_p & w_{pq} \\ w_{pq} & w_q \end{bmatrix}\begin{bmatrix} P - P_d \\ Q - Q_d \end{bmatrix}, \tag{2.58}$$

where w_p, w_q, and w_{pq} are design parameters satisfying $w_p > 0$ and $w_p w_q > w_{pq}^2$, so that $\left[\begin{smallmatrix} w_p & w_{pq} \\ w_{pq} & w_q \end{smallmatrix}\right]$ is a positive definite matrix. With these design parameters, one may specify how the differences $P - P_d$ and $Q - Q_d$ and their product $(P - P_d)(Q - Q_d)$ are penalized. Moreover, with U in (2.58) being a quadratic, positive definite function of $P - P_d$ and $Q - Q_d$, the smaller U is, the better the ultimate goal is achieved.

Having defined the performance measure U via (2.58), we next establish the following statement: if the subcontrollers in Sects. 2.4.1 and 2.4.2 are used with K chosen so that $A - BK$ has very fast eigenvalues, α chosen to be positive, and h chosen to satisfy (2.57), and if θ, ω_{rd}, β, V_w, P_d, and Q_d are all constants, then after a short transient, U may be expressed as a *known* function f_1 of r^2, θ, ω_{rd}, P_d, and Q_d, while r^2, in turn, may be expressed as an *unknown* function f_2 of ω_{rd}, β, and V_w, i.e.,

$$U = f_1(r^2, \theta, \omega_{rd}, P_d, Q_d), \tag{2.59}$$

$$r^2 = f_2(\omega_{rd}, \beta, V_w), \tag{2.60}$$

as shown in Fig. 2.3. To establish this statement, suppose the hypothesis is true. Then, after a short transient, it follows from (2.58) that U is a known function of P, Q, P_d, and Q_d; from (2.18)–(2.24), (2.29), and (2.30) that P and Q are known functions of φ, ω_r, u_1, and u_2; from (2.32) that φ is a known function of u_1 and u_2; from (2.34)

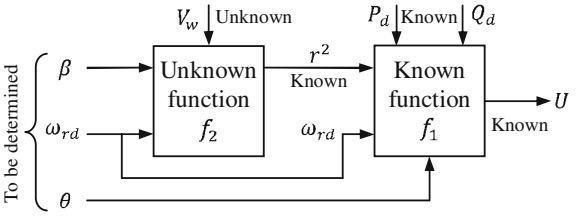


Fig. 2.3 Relationships among the performance measure U, the to-be-determined variables θ, ω_{rd}, and β, and the exogenous variables V_w, P_d, and Q_d

and (2.35) that u_1 and u_2 are known functions of r^2 and θ; and from Theorem 2.1 that $\omega_r = \omega_{rd}$. Thus, (2.59) holds with f_1 being known. Also, it follows from (2.54) and Theorem 2.1 that $r^2 = g(\omega_{rd}, \beta, V_w)$. Hence, (2.60) holds with f_2 being unknown.

Equations (2.59) and (2.60), which are represented in Fig. 2.3, suggest that U is a function of the to-be-determined variables θ, ω_{rd}, and β as well as the exogenous variables V_w, P_d, and Q_d. Given that the smaller U is the better, these to-be-determined variables may be chosen to minimize U. However, such minimization is difficult to carry out because although P_d and Q_d are known, V_w is not. To make matter worse, since f_1 is known but f_2 is not, the objective function is not entirely known. Somewhat fortunately, as shown in Fig. 2.3, θ affects U only through f_1 and not f_2. Therefore, θ may be chosen to minimize U for any given r^2, ω_{rd}, P_d, and Q_d, i.e.,

$$\theta = \arg\min_{x\in[-\pi,\pi)} f_1(r^2, x, \omega_{rd}, P_d, Q_d), \tag{2.61}$$

which is implementable since r^2, ω_{rd}, P_d, and Q_d are all known. Alternatively, θ may be chosen as in (2.61) but with a low-pass filter inserted to reduce possible chattering, such as a moving average filter, i.e.,

$$\theta(t) = \frac{1}{T_{ma}} \int_{t-T_{ma}}^{t} \arg\min_{x\in[-\pi,\pi)} f_1(r^2(\tau), x, \omega_{rd}(\tau), P_d(\tau), Q_d(\tau))d\tau, \tag{2.62}$$

where $T_{ma} > 0$ is the moving-average window size. With θ chosen as in (2.61), the minimization problem reduces from a three-dimensional problem to a two-dimensional one, depending only on ω_{rd} and β. Since the objective function upon absorbing θ is unknown and since V_w may change quickly, instead of minimizing U with respect to both ω_{rd} and β—which may take a long time—we decide to sacrifice freedom for speed, minimizing U only with respect to ω_{rd} and updating β in a relatively slower fashion, which will be described in Sect. 2.4.4.

The minimization of U with respect to ω_{rd} is carried out based on a gradient-like approach as shown in Fig. 2.4. To explain the rationale behind this approach, suppose β, V_w, P_d, and Q_d are constants. Then, according to (2.59)–(2.61), U is an unknown function of ω_{rd}. Because this function is not known, its gradient $\frac{\partial U}{\partial \omega_{rd}}$ at any ω_{rd} cannot be evaluated. To alleviate this issue, we evaluate U at two nearby ω_{rd}'s, use the two evaluated U's to obtain an estimate of the gradient $\frac{\partial U}{\partial \omega_{rd}}$, and move ω_{rd} along the direction where U decreases, by an amount which depends on the gradient estimate. This idea is illustrated in Fig. 2.4 and described precisely as follows: the desired rotor angular velocity $\omega_{rd}(t)$ is set to an initial value $\omega_{rd}(0)$ at time $t = 0$ and held constant until $t = T_1$, where T_1 should be sufficiently large so that both the electrical and mechanical dynamics have a chance to reach steady-state, but not too large which causes the minimization to be too slow. From time $t = T_1 - T_0$ to $t = T_1$, the average of $U(t)$, i.e., $\frac{1}{T_0}\int_{T_1-T_0}^{T_1} U(t)dt$, is recorded as the first value needed to obtain a gradient estimate. Similar to T_1, T_0 should be large enough so that small

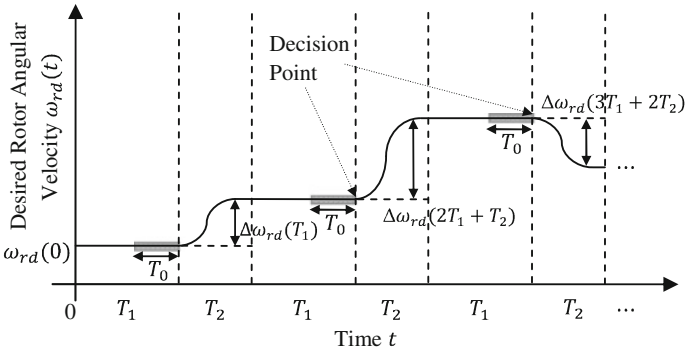


Fig. 2.4 Graphical illustration of the gradient-like approach

fluctuations in $U(t)$ (induced perhaps by a noisy V_w) are averaged out, but not too large which causes transient in the dynamics to be included. The variable $\omega_{rd}(t)$ is then changed gradually in an S-shape manner from $\omega_{rd}(0)$ at time $t = T_1$ to a nearby $\omega_{rd}(0)+\Delta\omega_{rd}(T_1)$ at $t = T_1+T_2$, where $\Delta\omega_{rd}(T_1)$ is an initial stepsize, and T_2 should be sufficiently large but not overly so, so that the transition in $\omega_{rd}(t)$ is smooth and yet not too slow. The variable $\omega_{rd}(t)$ is then held constant until $t = 2T_1 + T_2$, and the average of $U(t)$ from $t = 2T_1 + T_2 - T_0$ to $t = 2T_1 + T_2$, i.e., $\frac{1}{T_0}\int_{2T_1+T_2-T_0}^{2T_1+T_2} U(t)dt$, is recorded as the second value needed to obtain the gradient estimate. At time $t = 2T_1 + T_2$, the two recorded values are used to form the gradient estimate, which is in turn used to decide a new stepsize $\Delta\omega_{rd}(2T_1 + T_2)$ through

$$\Delta\omega_{rd}(2T_1 + T_2) = -\epsilon_1 \,\mathrm{sat}\left(\frac{\frac{1}{T_0}\int_{2T_1+T_2-T_0}^{2T_1+T_2} U(t)dt - \frac{1}{T_0}\int_{T_1-T_0}^{T_1} U(t)dt}{\epsilon_2 \Delta\omega_{rd}(T_1)}\right), \quad (2.63)$$

where $\epsilon_1 > 0$ and $\epsilon_2 > 0$ are design parameters that define the new stepsize $\Delta\omega_{rd}(2T_1 + T_2)$, and $\mathrm{sat}(\cdot)$ is the standard saturation function that limits $\Delta\omega_{rd}(2T_1 + T_2)$ to $\pm\epsilon_1$. Upon deciding $\Delta\omega_{rd}(2T_1 + T_2)$, $\omega_{rd}(t)$ is again changed in an S-shape manner from $\omega_{rd}(0) + \Delta\omega_{rd}(T_1)$ at $t = 2T_1 + T_2$ to $\omega_{rd}(0) + \Delta\omega_{rd}(T_1) + \Delta\omega_{rd}(2T_1 + T_2)$ at $t = 2T_1 + 2T_2$, in a way similar to the time interval $[T_1, T_1 + T_2]$. The process then repeats with the second recorded value from the previous cycle $[0, 2T_1+T_2]$ becoming the first recorded value for the next cycle $[T_1+T_2, 3T_1+2T_2]$, and so on. Therefore, with this gradient-like approach, ω_{rd} is guaranteed to approach a local minimum when β, V_w, P_d, and Q_d are constants, and track a local minimum when they are slow-varying.

Note that (2.58), (2.61), and (2.63) describe the *Polar Angle and Desired Rotor Angular Velocity Subcontroller* block in Fig. 2.2.

2.4.4 Blade Pitch Angle Subcontroller

As mentioned, in order to speed up the minimization, we have decided to minimize U only with respect to ω_{rd}, leaving the blade pitch angle β as the remaining undetermined variable. Given that an active power P that is larger than the rated value P_{rated} of the turbine may cause damage, we decide to use β to prevent P from exceeding P_{rated}, thereby protecting the turbine. Specifically, we let β be updated according to

$$\dot{\beta} = \begin{cases} 0, & \text{if } \beta = \beta_{\min} \text{ and } P < P_{\text{rated}}, \\ 0, & \text{if } \beta = \beta_{\max} \text{ and } P > P_{\text{rated}}, \\ -\epsilon_3(P_{\text{rated}} - P), & \text{otherwise}, \end{cases} \tag{2.64}$$

where $\epsilon_3 > 0$ is a design parameter that dictates the rate at which β changes. Note that with (2.64), β is guaranteed to lie in $[\beta_{\min}, \beta_{\max}]$. Moreover, when P is above (below) P_{rated}, β increases (decreases) if possible, in order to try to capture less (more) wind power, which leads to a smaller (larger) P.

Note that (2.64) describes the *Blade Pitch Angle Subcontroller* block in Fig. 2.2. Also note that the blade pitch angle subcontroller may be designed based on other considerations. For example, if the forecast of, say, the hourly average wind speed $\overline{V}_w$ is available, for blade protection β may be chosen as $\beta = F(\overline{V}_w)$ for some nondecreasing function $F : (0, \infty) \to [\beta_{\min}, \beta_{\max}]$.

2.5 Simulation Results

In this section, we demonstrate the effectiveness of the proposed controller through simulation in MATLAB using a realistic wind profile from a wind farm in Oklahoma. To describe the simulation settings and results, both the per-unit and physical unit systems will be used interchangeably.

The simulation settings are as follows: we consider the General Electric (GE) 1.5 MW turbine adopted by the Distributed Resources Library in MATLAB/Simulink, which has a base voltage of 575 V and a base frequency of 60 Hz. The values of the turbine parameters are: $\omega_s = 1$ pu, $R_s = 0.00706$ pu, $R_r = 0.005$ pu, $L_s = 3.071$ pu, $L_r = 3.056$ pu, $L_m = 2.9$ pu, $v_{ds} = 1$ pu, $v_{qs} = 0$ pu, $J = 10.08$ pu, $A = 4656.6\,\text{m}^2$, $R = 38.5$ m, $\beta_{\min} = 0°$, $\beta_{\max} = 30°$, and $C_f = 0.01$ pu. The C_p-surface adopted by MATLAB, which is taken from [51], is $C_p(\lambda, \beta) = c_1\left(\frac{c_2}{\lambda_i} - c_3\beta - c_4\right)e^{\frac{-c_5}{\lambda_i}} + c_6\lambda$, where $\frac{1}{\lambda_i} = \frac{1}{\lambda+0.08\beta} - \frac{0.035}{\beta^3+1}$, $c_1 = 0.5176$, $c_2 = 116$, $c_3 = 0.4$, $c_4 = 5$, $c_5 = 21$, and $c_6 = 0.0068$. The mechanical power captured by the wind turbine is $P_m(\text{pu}) = \frac{P_{\text{nom}} P_{\text{wind_base}}}{P_{\text{elec_base}}} C_p(\text{pu}) V_w(\text{pu})^3$, where $P_m(\text{pu}) = \frac{P_m}{P_{\text{nom}}}$, $P_{\text{nom}} = 1.5$ MW is the nominal mechanical power, $P_{\text{wind_base}} = 0.73$pu is the maximum power at the base wind speed, $P_{\text{elec_base}} = 1.5 \times 10^6/0.9$ VA is the base power of the electrical generator, $C_p(\text{pu}) = \frac{C_p}{C_{p_\text{nom}}}$, $C_{p_\text{nom}} = 0.48$ is the peak of the C_p-surface,

$V_w(\text{pu}) = \frac{V_w}{V_{w_\text{base}}}$, and $V_{w_\text{base}} = 12$ m/s is the base wind speed. Note that the maximum mechanical power, captured at the base wind speed, is 0.657 pu. The tip speed ratio is $\lambda(\text{pu}) = \frac{\frac{\omega_r(\text{pu})}{\omega_{r_\text{base}}}}{V_w(\text{pu})}$, where $\lambda(\text{pu}) = \frac{\lambda}{\lambda_{\text{nom}}}$, $\lambda_{\text{nom}} = 8.1$ is the λ that yields the peak of the C_p-surface, $\omega_{r_\text{base}} = 1.2$ pu is the base rotational speed, $\omega_r(\text{pu}) = \frac{\omega_r}{\omega_{r_\text{nom}}}$, and $\omega_{r_\text{nom}} = 2.1039$ rad/s is the nominal rotor angular velocity. For more details on these parameters and values, see the MATLAB documentation.

As for the proposed controller, we choose its parameters as follows: for the Rotor Voltages Subcontroller, we let the desired closed-loop eigenvalues of the electrical dynamics be at -5, $-10 \pm 5j$, and -15. Using MATLAB's place() function, the state feedback gain matrix $K = [K_1 \ K_2]^T$ that yields these eigenvalues is found to be

$$K = \begin{bmatrix} 5135.9 & 259.2 & 20.3 & 1.9 \\ -2676.7 & 4289.9 & -1.3 & 19.7 \end{bmatrix}.$$

Moreover, we let $\alpha = 5$ and $h = 17.5$ for the Electromagnetic Torque Subcontroller with Uncertainty Estimation; let $w_p = 10$, $w_q = 1$, $w_{pq} = 0$, $\epsilon_1 = 0.025$, $\epsilon_2 = 2$, $T_0 = 1$ s, $T_1 = 4$ s, and $T_2 = 6$ s and use (2.62) with $T_{ma} = 0.75$ s for the Polar Angle and Desired Rotor Angular Velocity Subcontroller; and let $\epsilon_3 = 3$ and $P_{\text{rated}} = 1$ pu for the Blade Pitch Angle Subcontroller.

The simulation results are as follows: we consider a scenario where the wind speed V_w is derived from actual wind profiles from a wind farm located in northwest Oklahoma, the desired active power P_d experiences large step changes, and the desired reactive power Q_d is such that the desired power factor PF_d is fixed at 0.995. As will be explained below, these values of P_d force the turbine to operate in both the MPT and PR modes and switch between them, under realistic wind profiles. Figures 2.5 and 2.6 show the simulation results for this scenario in both the per-unit and physical unit systems, wherever applicable. Note that in Fig. 2.5, for the first 1200 s during which P_d is unachievable at 1 pu, the turbine operates in the MPT mode and maximizes P, as indicated by the value of C_p approaching its maximum of 0.48 after a short transient (the turbine is initially at rest). At time 1200 s when P_d drops sharply from 1 pu to an achievable value of 0.35 pu, the turbine quickly reduces the value of C_p, accurately regulates P around P_d, and effectively rejects the "disturbance" V_w, thereby smoothly switches from the MPT mode to the PR mode. At time 2400 s when P_d goes from 0.35 pu back to 1 pu, the MPT mode resumes. Because V_w is strong enough at that time, P approaches P_d. Moreover, the moment P exceeds P_d (which is equal to P_{rated}), the blade pitch angle β increases in order to clip the power and protect the turbine. At time 2700 s when V_w becomes weaker, β returns to $\beta_{\min} = 0°$, thereby allowing the value of C_p to return to its maximum of 0.48 and P to be maximized. As can be seen from the figure, throughout the simulation, PF is maintained near PF_d, affected only slightly and relatively shortly by the random wind fluctuations. Moreover, the angular velocity ω_r tracks the desired time-varying reference ω_{rd} closely. As expected, the small S-shape variations in ω_{rd} resemble those in Fig. 2.4. Notice that similar observations can be made in Fig. 2.6,

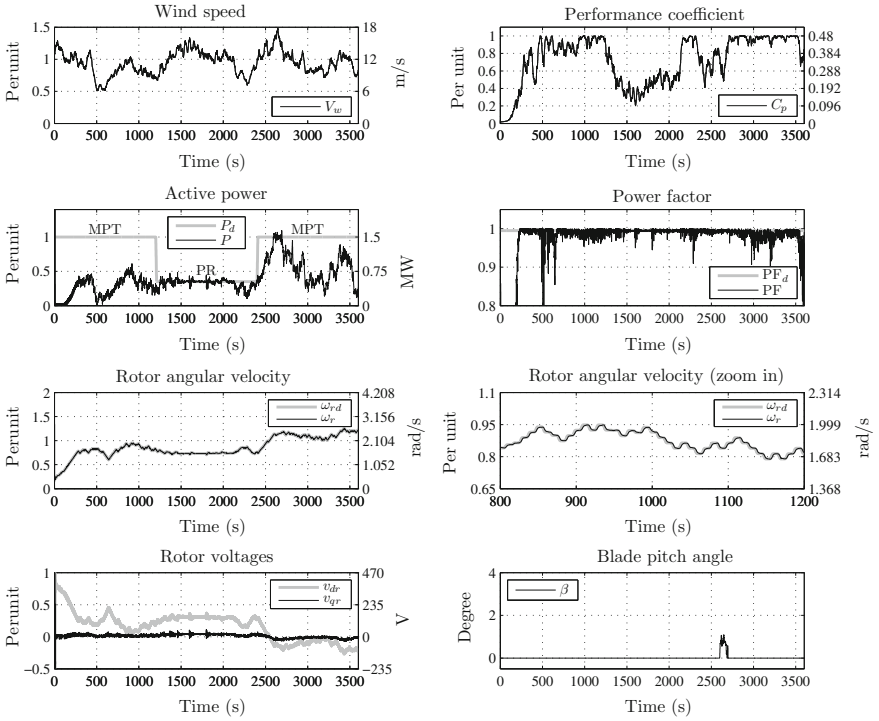


Fig. 2.5 Effective operation in both the MPT and PR modes and seamless switching between them under an actual wind profile from a wind farm located in northwest Oklahoma

which shows additional simulation results with a different wind profile and different desired active and reactive powers.

The above simulation results suggest that the proposed controller not only is capable of operating effectively in both the MPT and PR modes, it is also capable of switching smoothly between them—all the while not knowing the C_p-surface, air density, friction coefficient, and wind speed.

2.6 Concluding Remarks

In this chapter, we have described a mathematical model for variable-speed wind turbines employing DFIGs. Based on this model, we have utilized a number of control techniques—including feedback linearization, model order reduction, uncertainty estimation, and potential function minimization—to design a reconfigurable nonlinear dual-mode controller, which enables two most desirable operating modes of MPT and PR, while addressing other issues such as uncertainties in most of the

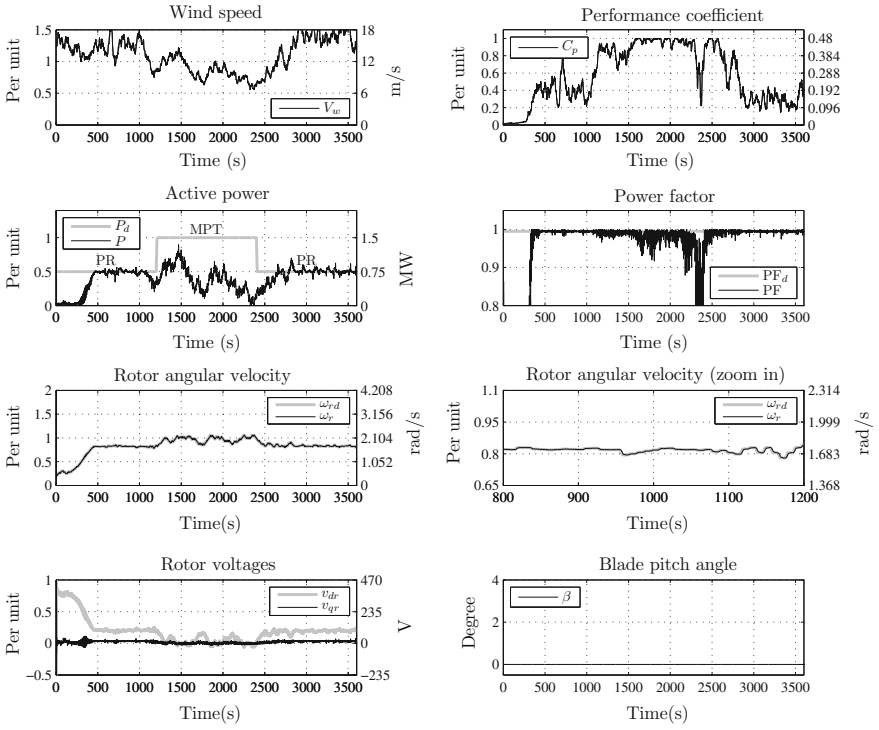


Fig. 2.6 Operation with a different wind profile and different desired active and reactive powers

model parameters. We have also demonstrated the effectiveness of this single-turbine controller through simulation with a realistic wind profile.

The work presented in this chapter, as well as those by many others, indicate that such reconfigurable controllers can expand the ability of active power control in meeting a number of rigid requirements on modern wind turbines. For example, when the above reconfigurable controller operates in the PR mode, the desired level of power output can be quickly reached and maintained, whenever wind is available. A controller equipped with such a PR mode allows the power produced from wind to become a source of secondary and tertiary controls for grid frequency support, or a source of up/down power balancing based on electricity market conditions. In addition, the PR mode offers turbines the flexibility to coordinate with other energy resources including storage and distributed generation.

Single-turbine control technologies have been at the center stage of research for many years. However, there are still a lot of challenges to overcome to fully meet the requirements of future power industry. For example, even for the well-known issue of using active power control to maintain the stability of grid frequency, it is not clear whether and to what extent wind farms can offer the full range of frequency support usually provided by conventional generation. Since electricity is not storable in large

quantities, at any given point in time, the amount of electricity produced must be equal to the amount consumed to maintain a constant grid frequency. When there is a dramatic imbalance between electricity production and consumption, frequency deviations occur, which may cause serious stability problems or even cascading failures. Due to constantly changing loads and inevitable events such as forced outages and natural disasters, a certain amount of reserves and fast generation support must be procured to stabilize and/or restore the frequency. Frequency support includes inertia response as well as primary, secondary, and tertiary controls that require different amount of power and response times. Although the above reconfigurable controller and those by others can relieve some of the concerns on secondary and tertiary controls, it is unclear whether they can address concerns regarding other frequency support.

Nevertheless, active power control at the turbine level is not the focus of this monograph. Instead, the concepts and functions of active power control introduced in this chapter set the stage for discussion of active power control at the wind farm level in subsequent chapters. Specifically, we will address a number of essential questions at the wind farm level such as: how should wind turbines be modeled to facilitate the design and analysis of wind farm controllers? How does a wind farm controller make the turbines cooperate to achieve a better performance? What are the potential of wind farm control in enhancing wind power sustainability, and what are the open challenges in this regard?

Springer

http://www.springer.com/978-3-319-39133-5

Control and Operation of Grid-Connected Wind Farms
Major Issues, Contemporary Solutions, and Open Challenges

Jiang, J.N.; Tang, C.Y.; Ramakumar, R.G.

2016, XIII, 139 p. 39 illus., 5 illus. in color., Hardcover
ISBN: 978-3-319-39133-5